

## *Supplemental Information for:*

### Molecular Investigation of the Multi-Phase Photochemistry of Fe(III)-Citrate in Aqueous Solution

Christopher P. West<sup>1</sup>, Ana C. Morales<sup>1</sup>, Jackson Ryan<sup>1</sup>, Maria M. Misovich<sup>1</sup>, Anusha P. S. Hettiyadura<sup>1</sup>, Felipe Rivera-Adorno<sup>1</sup>, Jay M. Tomlin<sup>1</sup>, Andrew Darmody<sup>2</sup>, Brittany N. Linn<sup>1</sup>, Peng Lin<sup>1,a</sup>, Alexander Laskin<sup>1,3\*</sup>

<sup>1</sup>Department of Chemistry, Purdue University, West Lafayette, IN, USA

<sup>2</sup>Department of Aeronautics and Aerospace Engineering, Purdue University, West Lafayette, IN

<sup>3</sup>Department of Earth, Atmospheric & Planetary Sciences, Purdue University, West Lafayette, IN, USA

<sup>a</sup>Now at California Air Resource Board (CARB), 1001 I Street, Sacramento, CA, USA

\*Correspondence to: [alaskin@purdue.edu](mailto:alaskin@purdue.edu)

## Contents

Appendix A. Transient Absorption (UV-visible) Optical Spectroscopy Experiments.....	S3
Figure S1. Description of photochemical and optical spectroscopy setup	
Appendix B. Chemical Actinometry Experiment & Calculations.....	S4
Figure S2. Single-wavelength absorbance plot of ferric-oxalate actinometric experiment.....	S5
Appendix C. Direct Infusion HRMS Parameters.....	S6
Appendix D. Formal Kinetic Model.....	S7
Appendix E. Calculation of Apparent Quantum Yields.....	S8
Appendix F. Conversion of Particle Counts to Lognormal Size Distribution.....	S9
Appendix G. Atmospheric Scaling Calculations.....	S10
Appendix H. TUV Model Calculations and Selected Parameters.....	S11
Figure S3. Quantification of Dissolved Fe(II).....	S12
Figure S4. Selected ion chromatograms (SICs) of Fe(III)-Citrate reactant complexes.....	S12
Figure S5. Direct infusion-mass spectrometry detection of Fe(III) Citrate complex ions.....	S13
Figure S6. MS <sup>2</sup> Structural characterization of Fe(III) Citrate complexes.....	S15
Figure S7. Selected ion chromatograms (SICs) of Fe(III)-Citrate and Fe(II)- Citrate.....	S16
Figure S8. <i>In Situ</i> FlowCam Nano images of colloidal particles.....	S17
Figure S9. Mass size distributions of detected colloids in unreacted and irradiated samples.....	S18
Figure S10. DI-HRMS spectrum of photoreacted sample under disruptive vs. non-disruptive conditions.....	S19
Figure S11. DI-HRMS spectrum of dissolved colloids in unreacted and photoreacted.....	S20
Figure S12. UV-visible spectrum of aqueous photolysis of Ferric Oxalate Complex.....	S21
Table S1. Summary Table of LC-PDA-HRMS molecular assignments.....	S22
Table S2. Summary Table of Fe(III)- Citrate complex ions acquired.....	
.....via direct infusion-HRMS.....	S32
Table S3. Summary Table of organic components identified in LC-ESI(-)-HRMS data.....	S33
References.....	S36



## Appendix B. Chemical Actinometry Experiment & Calculations

In the photolysis experiments described, the potassium ferrioxalate actinometer solution of volume,  $V$  is irradiated from the top in a standard  $b = 1.0$  cm quartz cuvette with a collimated beam of UV radiation with an illuminated cross-sectional area of cuvette ( $A = lw^2$ ). The absorption spectra are collected autonomously (procedure described in Appendix A). The spectral flux (photons  $\text{cm}^{-2} \text{s}^{-1}$ ) of the LED source by which photons are absorbed by the potassium ferrioxalate solution can be described with the following equations obtained from Lehoczki et al., 2013.<sup>1</sup>:

$$\frac{dC}{dt} = \frac{dA/dt}{\epsilon b} \quad (1)$$

$$F_{LED} \left( \frac{\text{Photons}}{\text{cm}^2 \text{ s}} \right) = \frac{\frac{dC}{dt} \cdot V}{\text{Area}} \times N_A \quad (2)$$

where  $dC/dt$  and  $dA/dt$  is the rate of change (slope) in the concentration and absorption,  $C$  and  $A$ , respectively. The line of best fit as described in Figure S2 obtains the slope,  $dA/dt$  ( $A.U. \text{ s}^{-1}$ ), which is converted to  $dC/dt$  using eq 1. For these experiments, a linear fit was used to obtain the measured photochemical rate constant,  $j$  ( $\text{s}^{-1}$ ), whereas  $dA/dt = -j \times [A]$ . The molar absorptivity,  $\epsilon$  of the solution ( $\epsilon_{Fe-Ox}$ ) at 390 nm is  $312 \pm 2 \text{ L mol}^{-1} \text{ cm}^{-1}$ . The rate of absorption by the actinometer solution (eq. 2) is calculated by plugging in eq.1 multiplied by the ratio of the volume irradiated ( $V = 0.003 \text{ L}$ ) and quantum yield,  $\phi$  ( $\phi \sim 1.26$ ), then divided by the cross-sectional area ( $Area$ ) of the beam ( $\sim 1.0 \text{ cm}^2$ ) and multiplied by Avogadro's constant ( $N_A$ ).

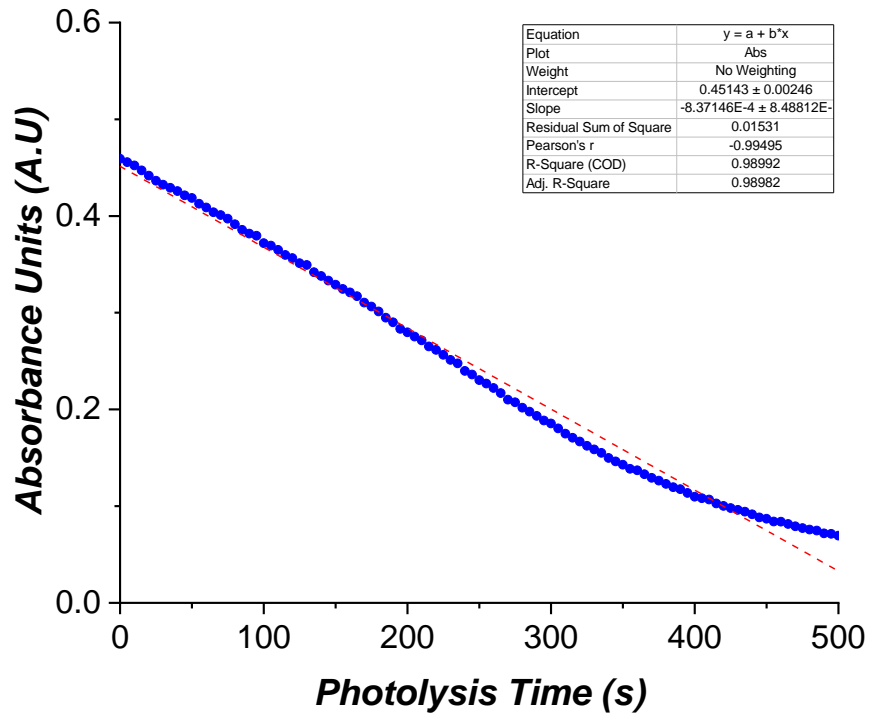


**Figure S2:** Averaged single wavelength absorbance at 390nm recorded in triplicate measurements of potassium ferrioxalate actinometer solution versus time (s) for LED driver setting used in study. Standard error for the y-intercept and slope are 0.026 and  $8.4 \times 10^{-6}$ , respectively.

The average spectral flux absorbed by the actinometer solution in these experiments is  $\sim 3.85 \times 10^{15}$  photons  $\text{cm}^{-2} \text{s}^{-1}$ .

## Appendix C. Direct Infusion HRMS Parameters

For direct infusion (DI) HRMS experiments, the funnel RF level was adjusted accordingly using 30 V and 80 V, to limit excessive in-source fragmentation and bias for low and high-molecular weight Fe-containing peaks and other species, respectively. Higher RF level offers higher transmission efficiencies of higher masses and vice versa, while the higher RF voltage may induce unwanted in-source fragmentation of fragile ions. Therefore, for LC-MS experiments, RF level was adjusted to 30 for screening of low-molecular weight species, while direct infusion experiments of water-soluble Fe<sup>III</sup>-citrate complex ions and dissolved colloids were adjusted to 80, to transmit the high molecular weight ions to MS detector. HRMS spectra for each of analyzed samples were acquired in negative ionization mode, whereas the colloids dissolved in *org-mix* were analyzed in both modes (pos mode analyzed only). Direct infusion ESI(+)-HRMS was chosen for analysis due to complexity of the sample matrix. All DI-ESI/HRMS, HPLC-PDA-ESI/HRMS data were acquired using Xcalibur software (Thermo Inc.). In all experiments, the HRMS was operated at  $m/\Delta m$  240,000 resolving power at 200 m/z, at a scan rate of 1.5 Hz in the full MS scan mode (100 – 1300 m/z range), whereas MS<sup>2</sup> experiments were operated at  $m/\Delta m$  120,000 resolving power, using 100 ms integration time. Targeted MS<sup>2</sup> experiments were performed via data independent acquisition (DIA) with an inclusion list of ions, which were mass selected and fragmented in the HCD collision cell at stepped CID voltage gradients with an optimal 35 eV collision energy and isolation window of ~ 0.4 m/z. The automatic gain control (AGC) target for all high resolution MS<sup>1</sup> and MS<sup>2</sup> experiments was set at 10<sup>5</sup>.

## Appendix D: Formal Kinetic Modeling

Three equations (eqn. 3-5) of the formal kinetic model calculate  $\alpha$ ,  $\beta$ ,  $\gamma$  fractions of the  $R$ ,  $I$  and  $P$  components based on the input values of photochemical rate constants,  $j_1$  and  $j_2$ . The latter were iteratively adjusted to provide a close match between the calculated profile of  $R+P$  and experimental values of  $MAC(\lambda)_{256\text{nm}}$  (Figure 1c in the main text).

$$\alpha = \frac{[R]}{[R_0]} = \exp^{-(j_1)t} \quad (1)$$

$$\beta = \frac{[I]}{[R_0]} = \frac{j_1}{j_2 - j_1} \times \exp^{-(j_1)t} - \exp^{(-j_2)t} \quad (2)$$

$$\gamma = \frac{[P]}{[R_0]} = 1 + \frac{1}{j_2 - j_1} \times [j_1 \exp^{(-j_2)t} - j_2 \exp^{(-j_1)t}] \quad (3)$$

From the fit of modeling results to experimental data, values of  $j_1 = 0.12 \text{ min}^{-1}$  and  $j_2 = 0.05 \text{ min}^{-1}$  were obtained. The obtained photochemical rate constants,  $j_i$ , were then converted to their laboratory half-lifetimes using eqn. 6.

$$\tau_{i, lab} = \frac{1}{j_{i, exp}} \quad (6)$$

Therefore, resulting in photochemical laboratory half-lifetime  $\tau_{i, lab}$  values of 8.3 and 20 min, respectively.

## Appendix E: Calculation of Apparent Quantum Yields

The apparent quantum yield ( $QY, \Phi$ ) for the photochemical degradation of Fe<sup>III</sup>-citrate was computed using eqn. 7-9 where:  $N_A$  is Avogadro's number,  $V$  is the irradiated solution volume,  $F_{LED}$  is the photon flux of the LED source,  $A_\sigma$  is the cross-sectional area of the exposed cuvette (1 cm<sup>2</sup>),  $t_{1/2}$  is the apparent half-life of the reference actinometer solution over measured range.  $[X]_0$  and  $[X]_{t_{1/2}}$  are the initial and half-life concentrations of Fe<sup>III</sup>-citrate, respectively.

$$QY(\Phi) = \frac{\# \text{ of Fe-Cit molecules reacted}}{\# \text{ of photons irradiated to solution}} \quad (7)$$

$$\# \text{ molecules reacted} = ([\text{Fe}^{\text{III}}\text{Cit}]_0 - [\text{Fe}^{\text{III}}\text{Cit}]_{t_{1/2}}) \times N_A \times V = 0.5 [\text{Fe}^{\text{III}}\text{Cit}]_0 \times N_A \times V \quad (8)$$

$$\# \text{ of photons irradiated to solution} = F_{LED} \times A_\sigma \times t_{1/2} \quad (9)$$

## Appendix F: Conversion of Particle Counts to Lognormal Mass Size Distribution

The FlowCam instrument records images of individual colloid particles and reports their 2D projected equivalent spherical diameters ( $D_p$ , size range 0.3 – 60  $\mu\text{m}$ ) as they pass focal point of the detector. Particle number size distributions (PSDs) were obtained by grouping the particle records into 8 per decade bins

$$\frac{\Delta N_i}{\Delta \log D_{p,i}} = \frac{\Delta N_i}{1/8} \quad (10)$$

where  $\Delta N_i$  is particle number concentration in bin  $i$  and  $D_{p,i}$  is the mean size of the corresponding bin. Then, the corresponding mass PSDs values were calculated as

$$\frac{\Delta M_i}{\Delta \log D_{p,i}} = \frac{\rho \times \frac{\pi}{6} D_{p,i}^3 \times \Delta N_i}{1/8} \quad (11)$$

where particle density  $\rho$  was assumed to be 1  $\text{g/cm}^3$ .

Experimental values of  $\Delta M_i / \Delta \log D_{p,i}$  were curve fit with a lognormal size distribution function of

$$\frac{dM}{d \ln D} = \frac{M_T}{\sqrt{2\pi} \ln \sigma_g} \exp \left[ -\frac{(\ln D - \ln \bar{D}_g M^2)^2}{2(\ln \sigma_g)^2} \right], \text{ where } \sigma_g = \sqrt{\frac{\sum_{i=1}^{N_{\text{bins}}} (y_{\text{meas}} - y_{\text{fit}})^2}{N_{\text{bins}} - 1}} \quad (12)$$

The mass loadings of the colloidal material ( $M_T$ ) were then calculated by integrating the lognormal fit of the data:

$$M_T = \int_0^{\infty} M(D_p) dD_p \quad (13)$$

## Appendix G: Atmospheric Scaling Calculations

Equivalent scaling of experimental values to real-world atmospheric conditions is achieved using eqn. 10 to obtain  $\tau_{i,eqv}$ . The calculated laboratory lifetime,  $\tau_{i,lab}$  values from eqn. 6 are incorporated into eqn. 10, followed by multiplication of the ratio of integrated fluxes ( $F_{lab}(\lambda) / F_{solar}(\lambda)_{24hr}$ ) from actinometer measurement ( $F_{lab}$ ) and TUV model ( $F_{solar}$ ) over the wavelength range of the absorbing irradiation (360-370 nm). Solar flux values are averaged over the 24 hr period on summer solstice June 20<sup>th</sup>, 2020, in the Los Angeles metropolitan and Jerusalem, Israel (Middle East) geographical areas. The scaling factor for the two cases are 3.65 and 3.8, respectively.

$$\tau_{i, eqv} = \tau_{i, lab} \times \frac{\int_{360nm}^{370 nm} F_{lab}(\lambda) d\lambda}{\int_{360nm}^{370 nm} F_{solar}(\lambda)_{24hr} d\lambda} \quad (14)$$

## Appendix H. Tropospheric UltraViolet Radiation (TUV) Model Calculation and Selected Parameters

Quick TUV Calculator ([www.acom.ucar.edu/Models/TUV/Interactive\\_TUV/](http://www.acom.ucar.edu/Models/TUV/Interactive_TUV/)) Selected Parameters:

Latitude/Longitude: 31.7683°N/ 35.2137°E (Jerusalem, Israel)

34.0522°N/118.2437° W (Los Angeles, California)

Date: June 20<sup>th</sup>, 2020

Time: 24hr average

Overhead Ozone Column: 300 du

Surface Albedo: 0.1

Ground Elevation: 0 kilometers Los Angeles; 1 kilometer Jerusalem, Israel

Clouds Optical Depth/Base/Top: 0.0/4.0/5.0

Aerosols Optical Depth/S-S Albedo/Alpha: 0.235/0.990/1.000

Sunlight Direct Beam/Diffuse Down/Diffuse Up: 1.0/1.0/1.0.

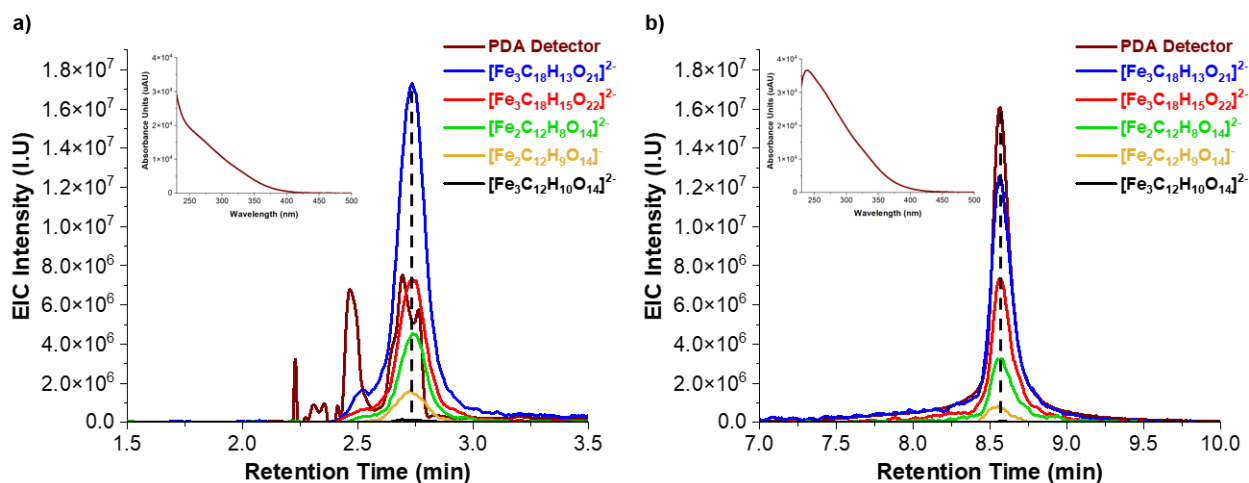
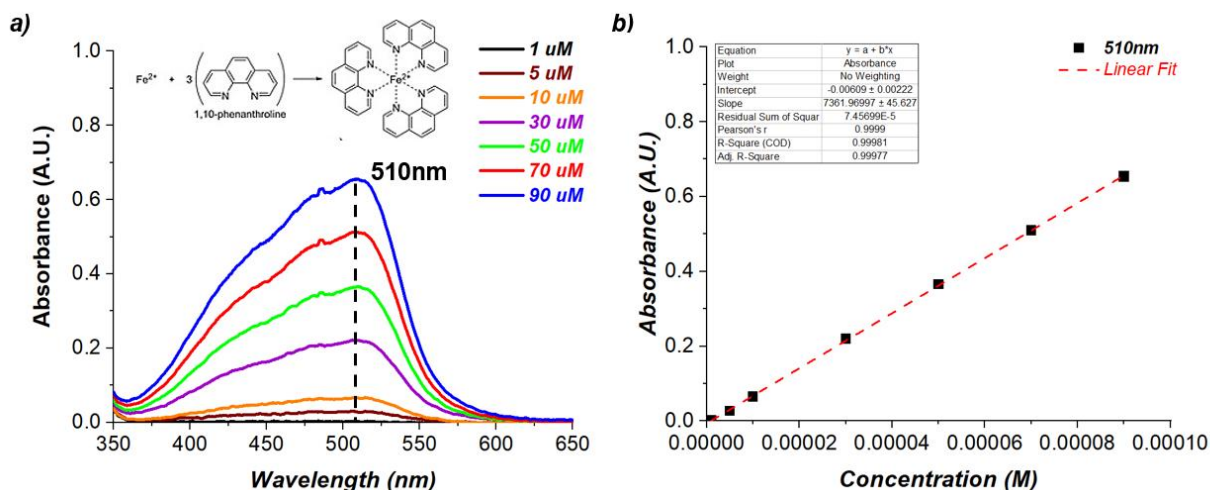


**Figure S4:** Extracted ion chromatograms (EIC) of select  $\text{Fe}(\text{III})$  citrate oligomeric complexes in the 0 min non-irradiated aliquot mixture eluting at a) 2.6min and b) 8.5min. Inset UV-visible absorption spectra (brown trace) integrated across the corresponding LC-PDA peak is shown. The LC-PDA peaks (brown) were centered and overlaid with individual ion chromatograms for visual comparison.

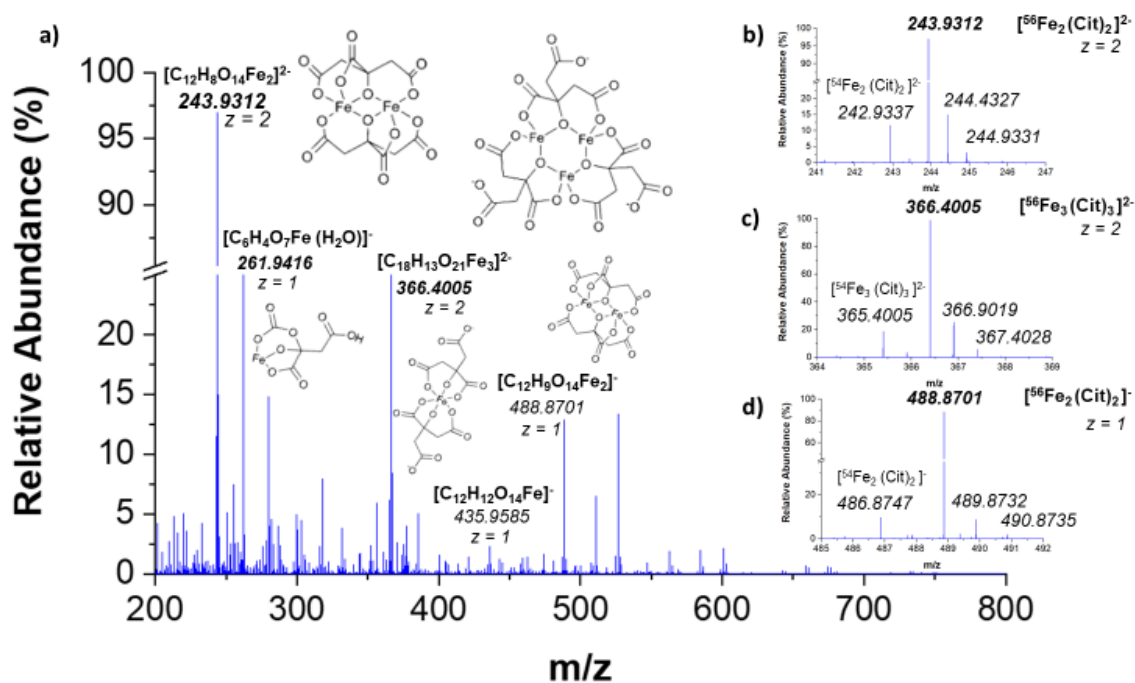


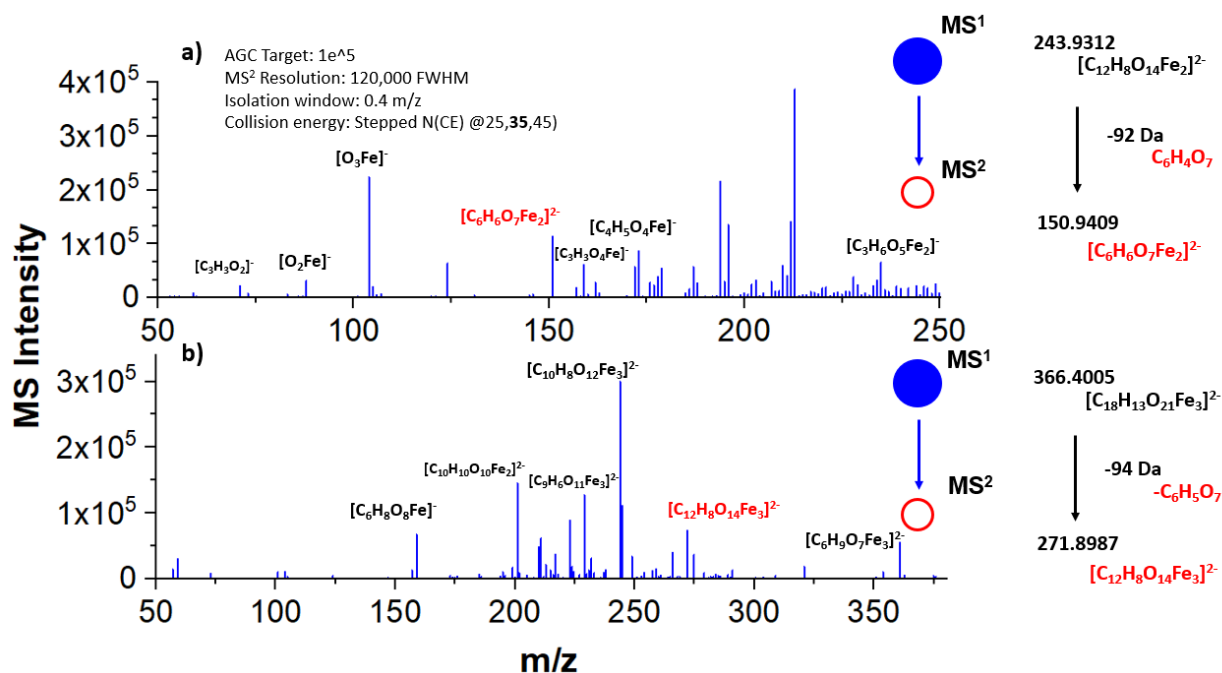
**Figure S5:** a) (-)ESI-HRMS spectra of 90 $\mu$ M Fe<sup>III</sup> perchlorate-citric acid aqueous solution along with notable Fe-citrate complex structures proposed in separate studies acquired on FT-Orbitrap HF-X instrument. Normalized HRMS spectra representing isotope distribution for b) dinuclear, c) trinuclear iron, and d) dinuclear iron Fe<sup>III</sup> citrate complex ions (1:1 M:L).

The prepared aqueous solution of Fe<sup>III</sup> perchlorate hydrate salt and citric acid in a 1:1 (90 $\mu$ M:90 $\mu$ M) molar ratio of metal and ligand (M:L) were analyzed via direct infusion electrospray ionization (ESI)-HRMS operated in the negative ionization mode to screen and detect for all deprotonated ions characteristic of the Fe<sup>III</sup>-citrate complexes. ESI-HRMS is particularly sensitive method to screen for polar carboxylic acids, carbonyls, and especially metallo-organic complexes incorporating metals such as: iron (Fe), nickel (Ni), zinc (Zn), manganese (Mn), copper (Cu) and metal salts incorporating mercury (Hg), lead (Pb), bismuth (Bi), strontium (Sb), and Arsenic (As).<sup>4,5</sup> ESI-MS has been used in previous studies to characterize metal complexes in biological and environmental matrices,<sup>6,7</sup> as well as to study the protonation states of Fe(III) and Fe(II) citrate complexes in aqueous solution.<sup>4,8,9</sup> Figure S5a illustrates the DI-ESI(-)-HRMS spectrum of the Fe<sup>III</sup> perchlorate: citric acid solution. In addition, we injected the ferric citrate reagent used in the main text to compare with the referenced MS spectrum in Figure S5 and literature reported ions. In our work, the measured pH of the freshly prepared 1:1 M:L ferric citrate standard reagent and

Fe<sup>III</sup> perchlorate-citrate solution was pH ~ 6.86 and ~ 4.94, respectively, all before adding 20% methanol prior to HRMS analysis, as recommended in the literature.<sup>8,9</sup>

In this dataset, the most abundant molecular ion corresponding to mono-deprotonated citric acid (H<sub>2</sub>Cit; C<sub>6</sub>H<sub>8</sub>O<sub>7</sub>; m/z = 191.1045) is observed; however, to obtain targeted analysis of Fe(III) citrate complexes, we screened for analytes in the 200–1300 m/z MS range, similar to the works of Silva and Gautier-Luneau.<sup>8,9</sup> Additional details of the HRMS peak assignments is described in Table S1. The results of Figure S5a reveal abundant detection of numerous Fe(III) citrate oligomeric complexes in different stoichiometric Fe: citrate M:L ratios. The most abundant molecular ions are the multiply charged dinuclear dicitrate complexes, [<sup>56</sup>Fe<sub>2</sub>C<sub>12</sub>H<sub>8</sub>O<sub>14</sub>]<sup>2-</sup> (m/z = 243.93 Da) and [<sup>56</sup>Fe<sub>2</sub>C<sub>12</sub>H<sub>9</sub>O<sub>14</sub>]<sup>-</sup> (m/z = 488.87 Da) and the trinuclear tricitrate complexes, [<sup>56</sup>Fe<sub>3</sub>C<sub>18</sub>H<sub>13</sub>O<sub>21</sub>]<sup>2-</sup> (m/z = 366.40 Da) and [<sup>56</sup>Fe<sub>3</sub>C<sub>18</sub>H<sub>15</sub>O<sub>22</sub>]<sup>2-</sup> (m/z = 375.40 Da) observed. Additional molecular ions resembling mononuclear ferric citrate complexes were identified, including [<sup>56</sup>FeC<sub>6</sub>H<sub>4</sub>O<sub>7</sub> (H<sub>2</sub>O)]<sup>-</sup> (m/z = 261.94 Da). However, very few of those were observed in lower abundance relative to the largest HRMS signal. For example, mononuclear dicitrate complexes, [<sup>56</sup>FeC<sub>12</sub>H<sub>11</sub>O<sub>14</sub>]<sup>2-</sup> (m/z = 217.47 Da) and [<sup>56</sup>FeC<sub>12</sub>H<sub>12</sub>O<sub>14</sub>]<sup>-</sup> (m/z = 435.95 Da), observed in the 1:2 stoichiometric Fe: Cit ratio were detected at approximately 10% of ESI-HRMS signal. This experimental observation is further supported by speciation models of ferric citrate at acidic and near-neutral pH conditions, whereby 1:2 Fe: citrate complexation is very low.<sup>9</sup> Other Fe-citrate ions comprising the 3:4 and 4:3 M:L complexes in the form of double charged ions are [<sup>56</sup>Fe<sub>3</sub>C<sub>24</sub>H<sub>21</sub>O<sub>28</sub>]<sup>2-</sup> (m/z = 462.41 Da) and [<sup>56</sup>Fe<sub>4</sub>C<sub>21</sub>H<sub>12</sub>O<sub>22</sub>]<sup>3-</sup> (m/z = 279.90 Da), respectively. These complexes resemble much larger structures than the 1:1, 1:2, 2:2, and 3:3 Fe: citrate species previously discussed. For the pH range (5-7 pH units) in our samples, binuclear and trinuclear ferric citrate complexes appear to influence the overall chemical composition of the sample at the specified pH ranges. Full description of Fe-citrate complex ions detected are reported in Table S2 for the two Fe-citrate systems. Overall, the HRMS results indicate that molecular speciation of ferric citrate is dominated by large oligomeric complexes in the binuclear and trinuclear Fe coordination states. The structures shown in Figure S5a are representative solid-state structures obtained in previous X-ray crystallographic measurements.<sup>8,9</sup> However tandem mass spectrometry studies detailing the structures in the gas-phase have not been extensively studied. The measured isotope distribution shown in Figures S5b-d for the di- and trinuclear Fe-citrate complexes

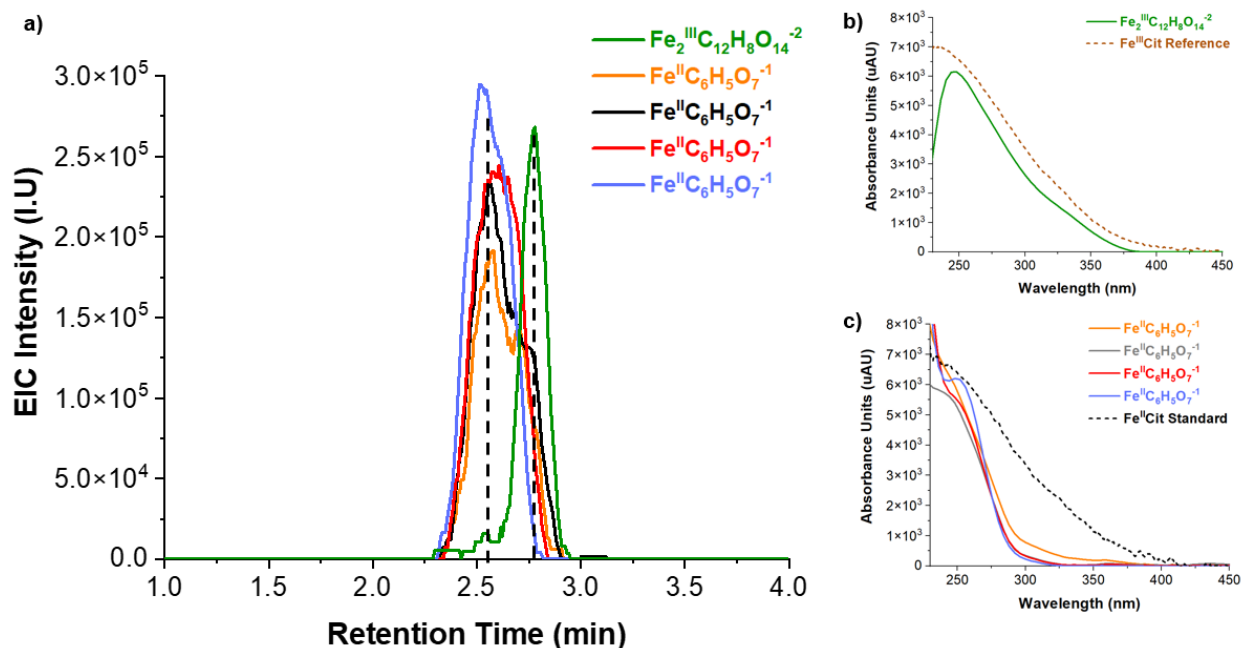
confirmed the presence of the  $^{54}\text{Fe}$  (5.8%),  $^{56}\text{Fe}$  (91.7%),  $^{57}\text{Fe}$  (2.1%), and  $^{58}\text{Fe}$  (0.3%) isotopes as compared with theoretical isotopic model.



**Figure S6:** MS<sup>2</sup> spectra obtained for a)  $[\text{Fe}_2\text{C}_{12}\text{H}_8\text{O}_{14}]^{2-}$  and b)  $[\text{Fe}_3\text{C}_{12}\text{H}_8\text{O}_{14}]^{2-}$  representing dinuclear and trinuclear  $\text{Fe}^{\text{III}}$ -citrate complex ions in the negative ESI mode.

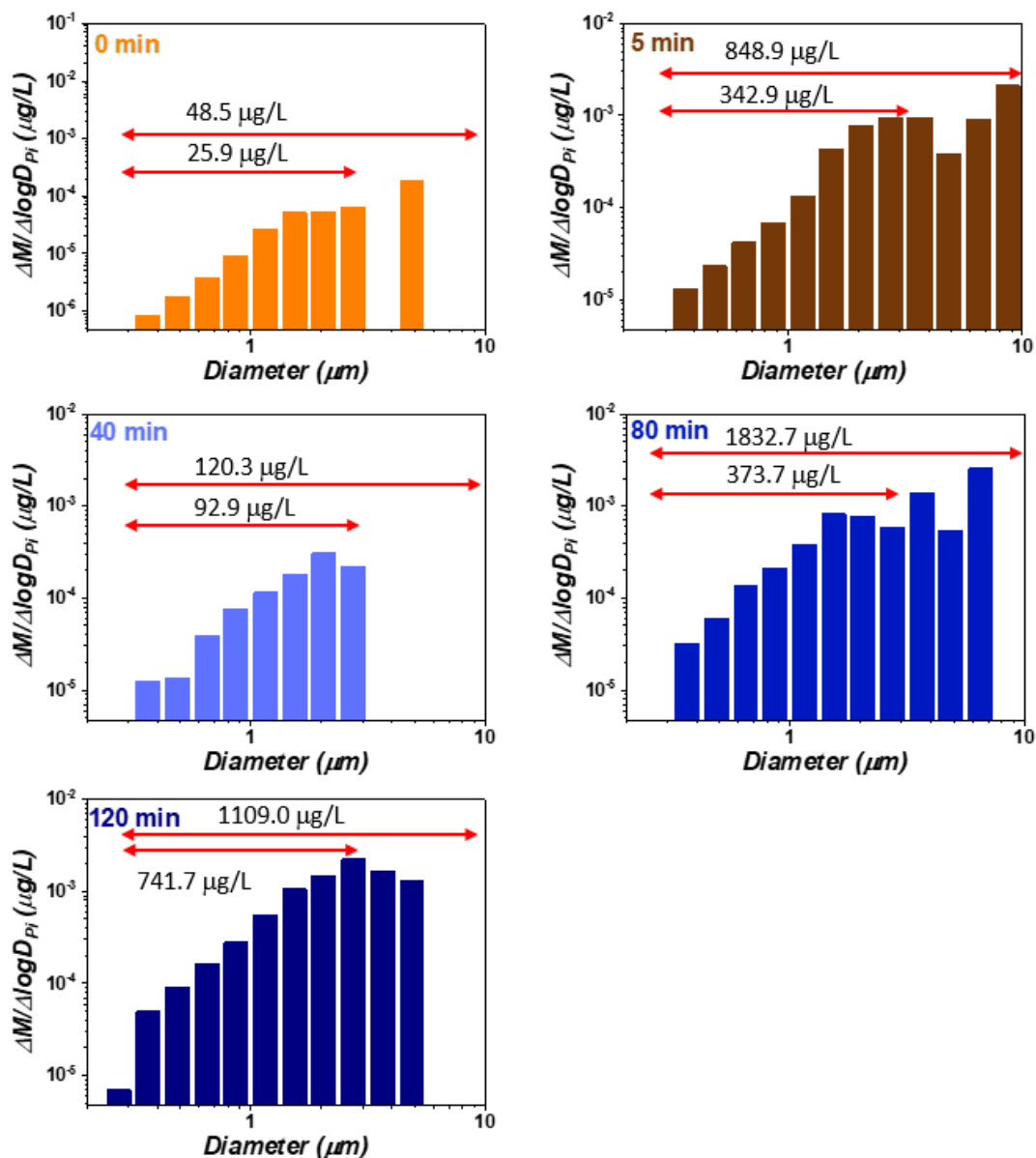
We employ tandem mass spectrometric (MS<sup>2</sup>) analysis via data-independent acquisition (DIA) and parallel reaction monitoring (PRM) with an inclusion list of select ferric citrate complex ions for structural determination and identification. The DIA and PRM MS<sup>2</sup> modes reveal similar fragmentation spectrums, therefore we chose to discuss the DIA-MS<sup>2</sup> results in this section and comparison between two methods in the SI file. The fragmentation of metal-ligand complexes in complex biological samples has been used in previous studies using high-energy collisional dissociation (HCD) to study the metal ion release from anionic complexes.<sup>7,10</sup> HCD has been demonstrated as a useful application for obtaining detailed elemental composition and structural information of metal organics.<sup>10</sup> Figure S6 represents the DIA-MS<sup>2</sup> spectrum of the fragmented ions for the dinuclear and trinuclear Fe-citrate complex ions characterized. The dinuclear dicitrate complex ion  $[\text{Fe}_2\text{C}_{12}\text{H}_8\text{O}_{14}]^{2-}$  (m/z = 243.93 Da), upon HCD, undergoes neutral loss of citric acid to yield dinuclear monocitrate complex ion  $[\text{Fe}_2\text{C}_6\text{H}_6\text{O}_7]^{2-}$  (m/z = 150.94 Da). Additionally, the

trinuclear tricitrate complex  $[^{56}\text{Fe}_3\text{C}_{18}\text{H}_{13}\text{O}_{21}]^{2-}$  ( $m/z = 366.40$  Da) also fragments upon HCD into the trinuclear dicitrate complex ion  $[^{56}\text{Fe}_3\text{C}_{12}\text{H}_8\text{O}_{14}]^{2-}$  ( $m/z = 271.89$  Da) following the neutral loss of one citric acid molecule. Additional fragment ions detected in the  $\text{MS}^2$  spectra represent characteristic Fe fragment ions. The  $\text{MS}^2$  experiments in this study suggest the identified analytes in the sprayed sample are Fe-organic complexes. This level of analysis provides experimental confirmation of Fe-organic complexes in aqueous solution.

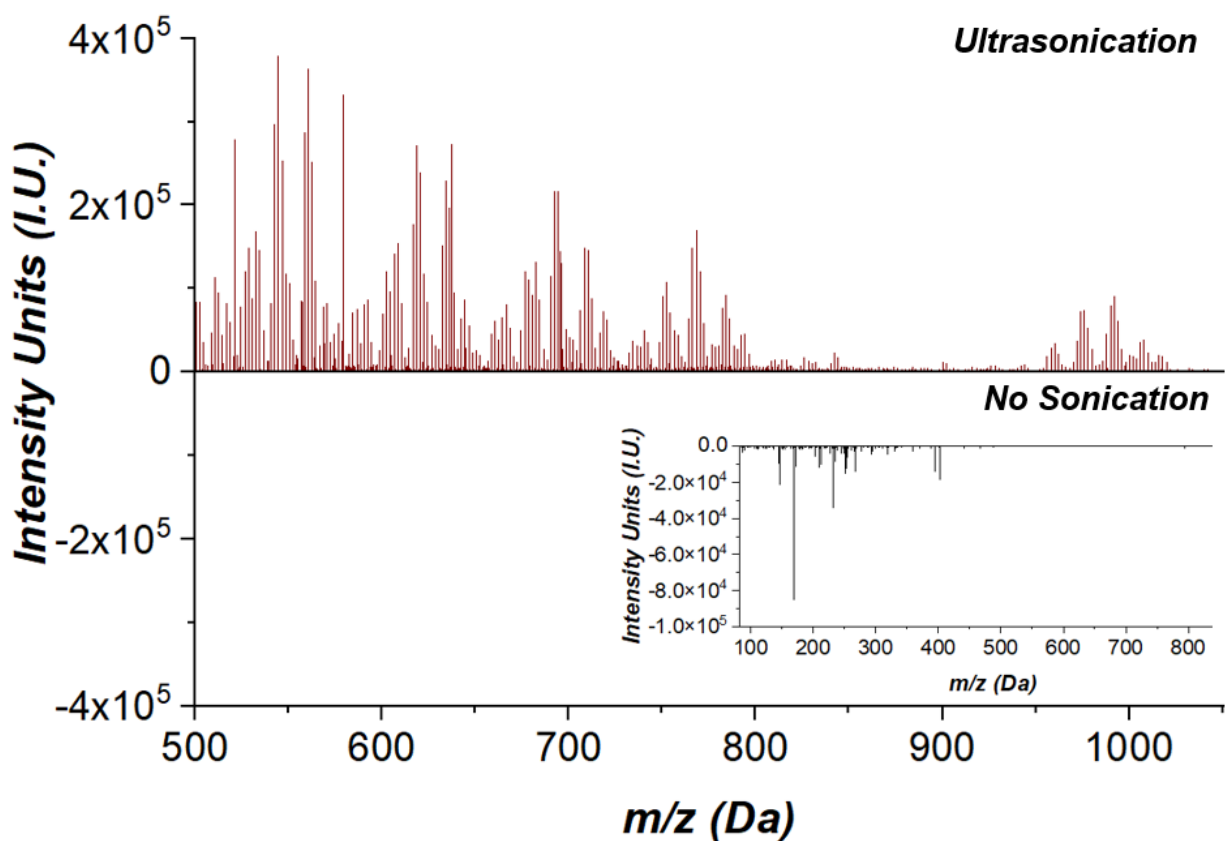


**Figure S7:** a) Extracted ion chromatograms (EIC) of select Fe(III) citrate in the 5 min photolyzed aliquot mixture as  $[\text{Fe}^{\text{III}}_2\text{C}_{12}\text{H}_8\text{O}_{14}]^{2-}$  (green). EIC's for Fe<sup>II</sup> citrate species at the 5 (orange), 40 (black), 80 (red), and 120 (light blue) min irradiated mixtures. Reference bulk UV-visible spectra are shown for b) Fe(III)-citrate (brown dotted lines) and c) Fe(II)-citrate standard (black dotted lines) prepared in the lab (dashed line) along with the UV-Visible spectra of the individual Fe<sup>III/II</sup>-citrate LC-PDA-HRMS features.

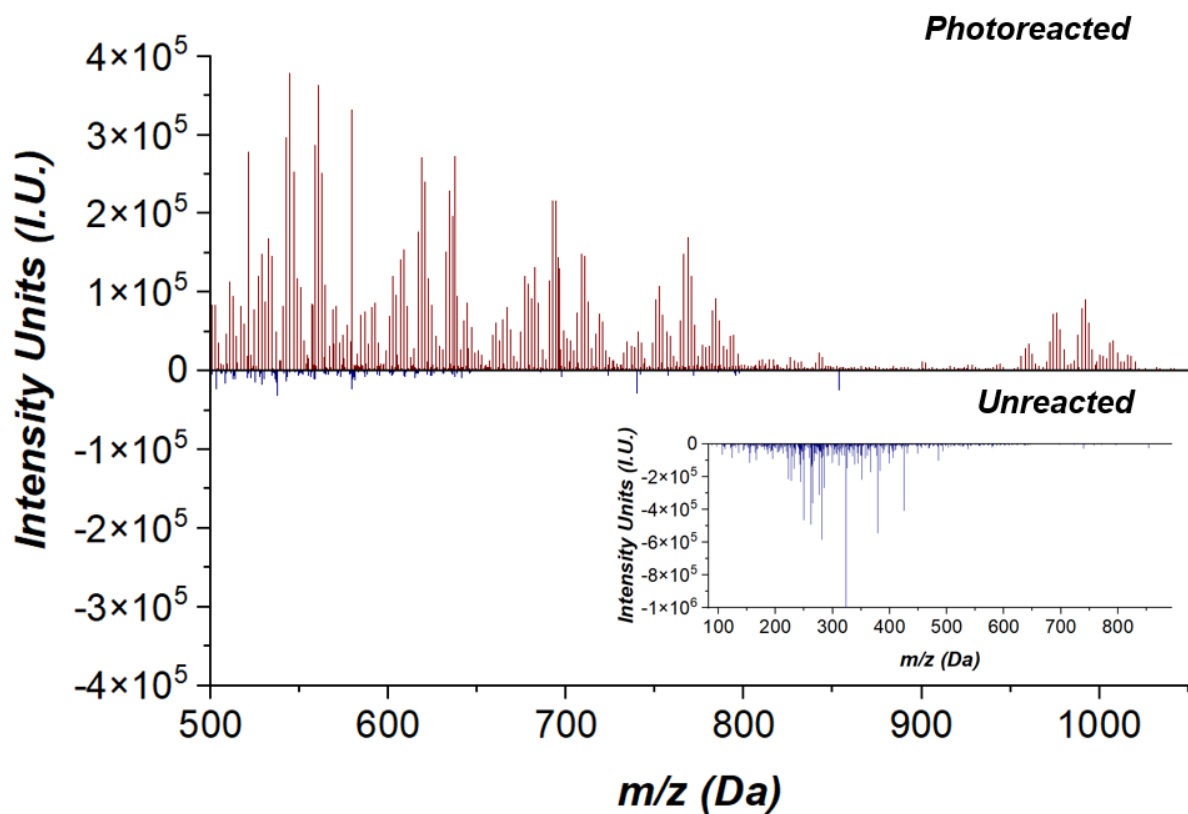




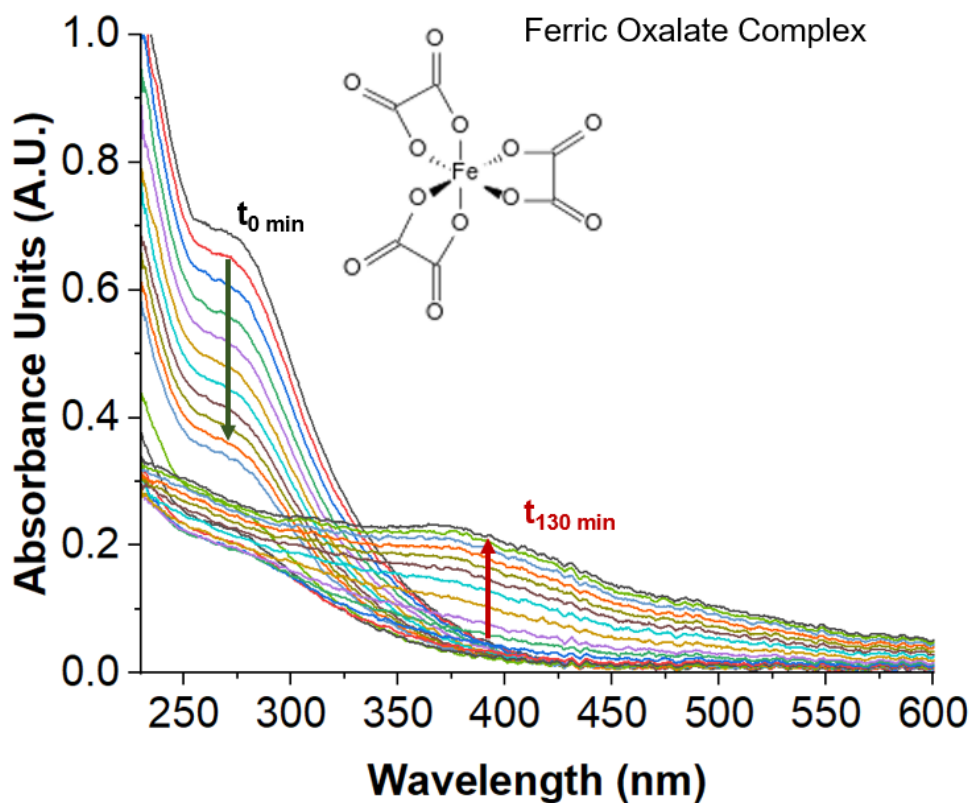
**Figure S9:** Mass size distributions of colloids detected in the unreacted, 5, 40, 80, and 120 min irradiated samples. The upper and lower limit mass loadings are reported for the 40, 80, and 120 min irradiated samples to account for the largest particles sparsely detected in the samples.



**Figure S10:** DI-ESI(+)/HRMS spectrum of dissolved colloidal material probed at the 120 min photolysis time following ultrasonication (top panel) and no sonication procedures (bottom panel). The photoreacted sample (bottom panel) was sprayed into HRMS without sonication and dissolution procedures, illustrating differences in the measured compositions following sample treatment.

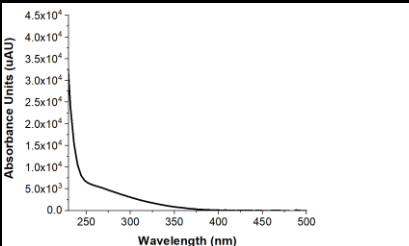
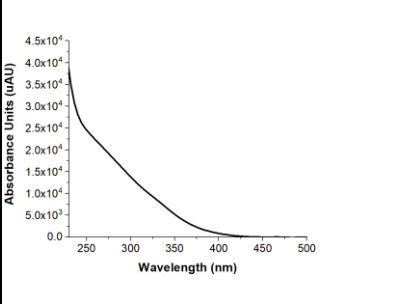
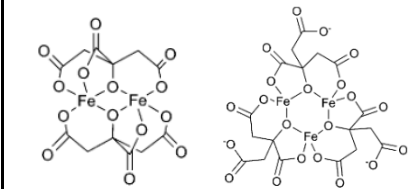
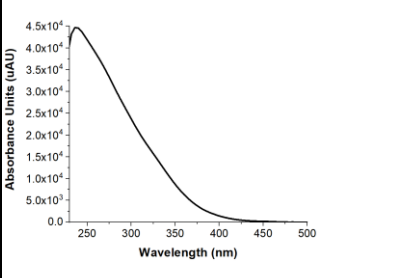
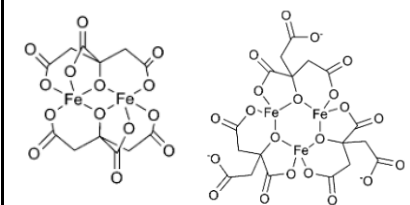


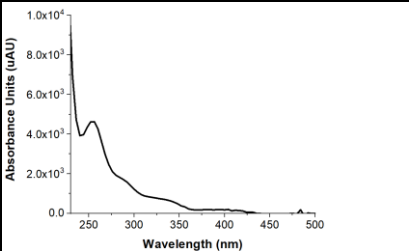
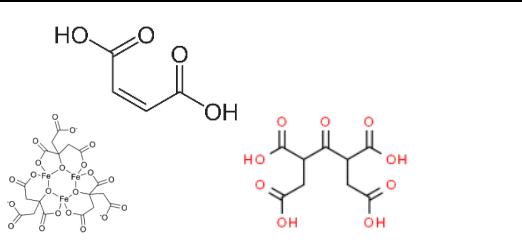
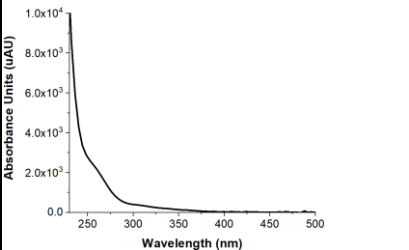
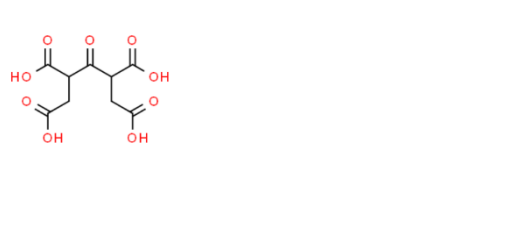
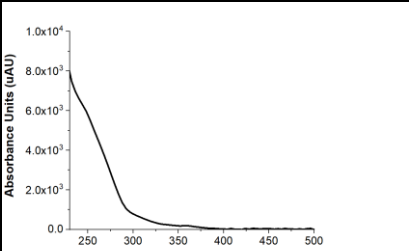
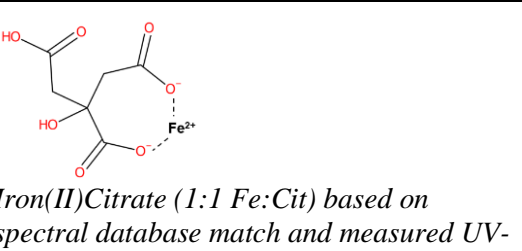
**Figure S11:** DI-ESI(+)/HRMS spectrum of dissolved colloidal material probed at the 120min photolysis time (top panel) and unreacted Fe(III)-citrate sample (bottom panel) following the same dissolution procedures.

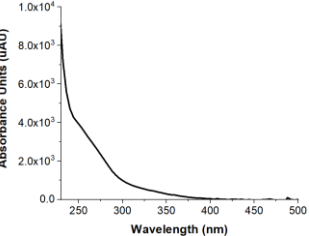
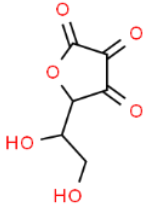
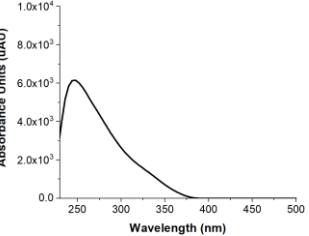
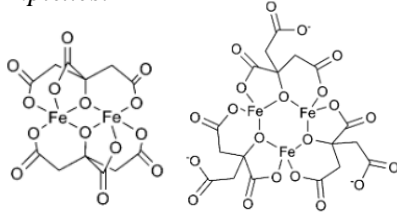
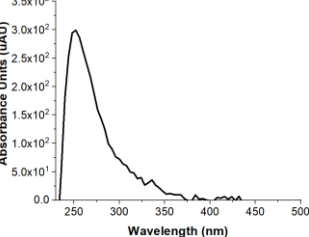
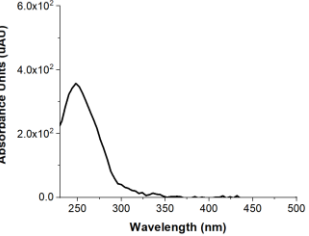
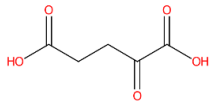


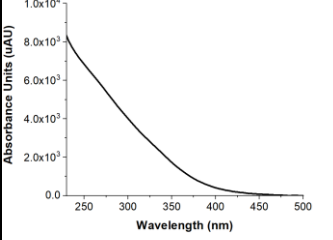
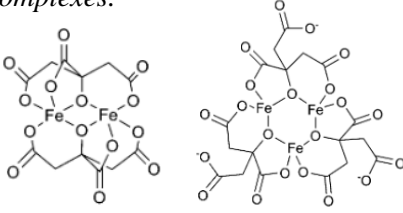
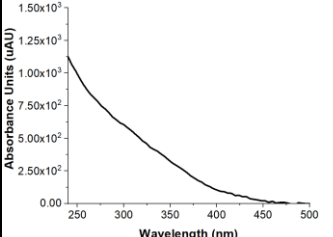
**Figure S12:** UV-visible absorption spectra illustrating the aqueous photolysis of ferric oxalate complex over the 130 min period of the photolysis. UV-vis were acquired using similar procedure in the experimental setup; however the light intensity was adjusted to lower dial setting to slow down reaction kinetics. The presumed degradation of ferric oxalate complex at ~270nm is observed over the 0-10 min period, followed by build-up in signal at ~370nm over the follow-up period 20 – 130min of the photolysis. The measured light extinction is extended beyond 500nm visible region.

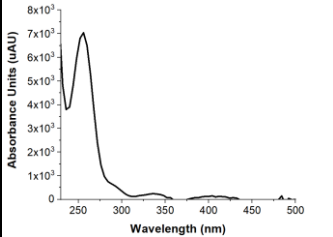
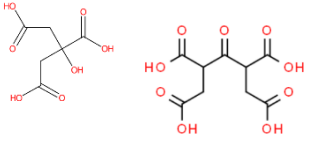
**Table S1:** LC retention times (RT), UV-visible spectra, experimental m/z, assigned elemental formulas, mass error, and proposed structures of the major identified chromophores in each of the photolysis steps (0, 5, 40, 80, 120 min).

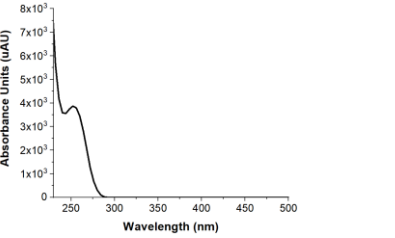
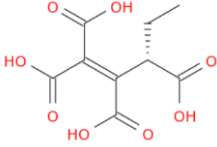
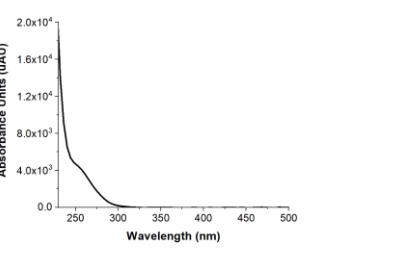
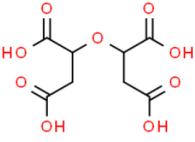
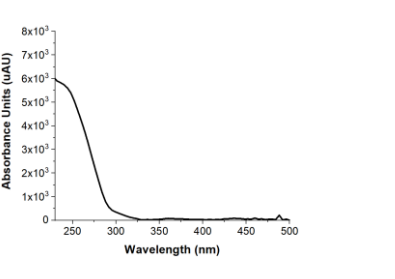
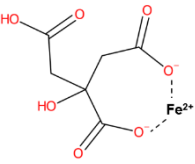
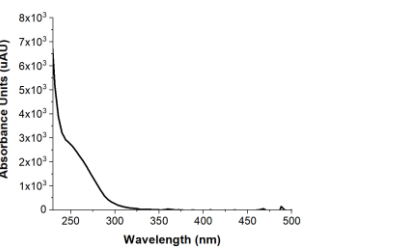
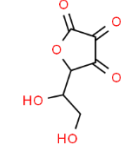
PDA RT (min)	UV-Vis Spectrum	m/z	Ionic, Neutral Formula	Mass Error (ppm)	Proposed Structure & Description
		(-) mode			
<i>Unreacted</i>					
Un2.39		159.972	$\text{Fe}_2^{\text{III}}\text{C}_{11}\text{H}_{12}\text{O}_4^{-2}$	1.875	Based on the high mass accurate measurement and detection of the $[\text{}^{54}\text{Fe}_2(\text{III})\text{C}_{11}\text{H}_{12}\text{O}_4]^{2-}$ isotope recorded as the molecular ion.
2.61		366.4006 375.4063 243.9313 488.8700 271.8991	$\text{Fe}_3^{\text{III}}\text{C}_{18}\text{H}_{13}\text{O}_{21}^{-2}$ $\text{Fe}_3^{\text{III}}\text{C}_{18}\text{H}_{15}\text{O}_{22}^{-2}$ $\text{Fe}_2^{\text{III}}\text{C}_{12}\text{H}_8\text{O}_{14}^{-2}$ $\text{Fe}_2^{\text{III}}\text{C}_{12}\text{H}_9\text{O}_{14}^{-1}$ $\text{Fe}_3^{\text{III}}\text{C}_{12}\text{H}_{10}\text{O}_{14}^{-2}$	0.689 0.533 0.152 0.466 0.345	 Iron(III)-citrate (2:2 ; 3:3 Fe: cit) oligomeric complexes based on previous literature, Fe isotope distribution, and optical signal. <sup>9,11</sup>
8.48		366.4006 375.4063 243.9313 488.8700 271.8989	$\text{Fe}_3^{\text{III}}\text{C}_{18}\text{H}_{13}\text{O}_{21}^{-2}$ $\text{Fe}_3^{\text{III}}\text{C}_{18}\text{H}_{15}\text{O}_{22}^{-2}$ $\text{Fe}_2^{\text{III}}\text{C}_{12}\text{H}_8\text{O}_{14}^{-2}$ $\text{Fe}_2^{\text{III}}\text{C}_{12}\text{H}_9\text{O}_{14}^{-1}$ $\text{Fe}_3^{\text{III}}\text{C}_{12}\text{H}_{10}\text{O}_{14}^{-2}$	0.307 0.134 0.152 0.998 1.530	 Iron(III)-citrate (2:2 ; 3:3 Fe: cit) oligomeric complexes. <sup>9,11</sup>

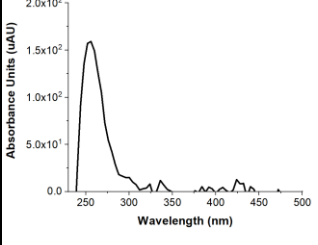
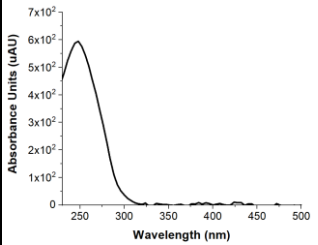
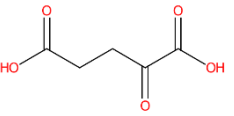
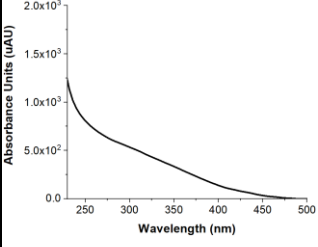
<i>PDA RT (min)</i>	<i>UV-Vis Spectrum</i>	<i>m/z</i>	<i>Ionic, Neutral Formula</i>	<i>Mass Error (ppm)</i>	<i>Proposed Structure &amp; Description</i>
		<i>(-) mode</i>			
<b>5 min Photolysis</b>					
2.24		115.0038 261.0253 366.4001	C <sub>4</sub> H <sub>4</sub> O <sub>4</sub> C <sub>9</sub> H <sub>10</sub> O <sub>9</sub> Fe <sub>3</sub> <sup>III</sup> C <sub>18</sub> H <sub>13</sub> O <sub>21</sub> <sup>-2</sup>	0.853 0.938 -0.512	
2.37		261.0253	C <sub>9</sub> H <sub>10</sub> O <sub>9</sub>	1.054	
2.44		244.9396	Fe <sup>II</sup> C <sub>6</sub> H <sub>5</sub> O <sub>7</sub> <sup>-1</sup>	2.009	 <i>Iron(II)Citrate (1:1 Fe: Cit) based on spectral database match and measured UV-visible spectra.<sup>12</sup></i>

2.6		255.0180 242.9818 173.0093	$\text{Fe}^{\text{II}}\text{C}_6\text{H}_{15}\text{O}_7^{-1}$ $\text{Fe}^{\text{II}}\text{C}_4\text{H}_{11}\text{O}_8^{-1}$ $\text{C}_6\text{H}_6\text{O}_6$	2.046 3.199 0.122	
2.7		366.4006 375.4063 243.9313	$\text{Fe}_3^{\text{III}}\text{C}_{18}\text{H}_{13}\text{O}_{21}^{-2}$ $\text{Fe}_3^{\text{III}}\text{C}_{18}\text{H}_{15}\text{O}_{22}^{-2}$ $\text{Fe}_2^{\text{III}}\text{C}_{12}\text{H}_8\text{O}_{14}^{-2}$	0.116 0.213 0.439	<i>Iron(III)-citrate (2:2 ; 3:3 Fe: cit) oligomeric complexes.<sup>9,11</sup></i> 
3.12		211.0281 197.0125	$\text{Fe}^{\text{II}}\text{C}_5\text{H}_{15}\text{O}_5^{-1}$ $\text{Fe}^{\text{II}}\text{C}_4\text{H}_{13}\text{O}_5^{-1}$	3.2 3.2	
6.22		255.0180 211.0281 145.0142	$\text{Fe}^{\text{II}}\text{C}_6\text{H}_{15}\text{O}_7^{-1}$ $\text{Fe}^{\text{II}}\text{C}_5\text{H}_{15}\text{O}_5^{-1}$ $\text{C}_5\text{H}_6\text{O}_5$	2.713 3.2 0.252	

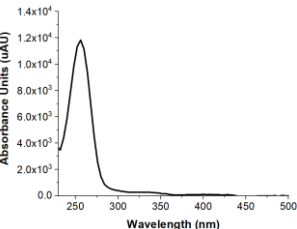
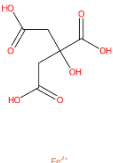
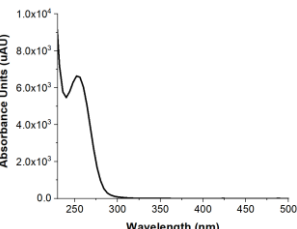
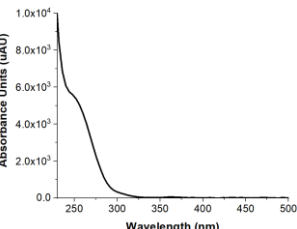
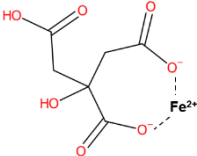
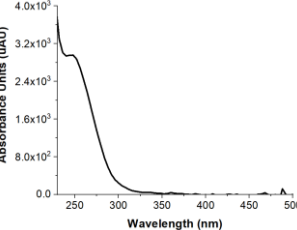
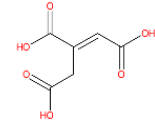
8.58		366.4006 375.4063 243.9313	$\text{Fe}_3^{\text{III}}\text{C}_{18}\text{H}_{13}\text{O}_{21}^{-2}$ $\text{Fe}_3^{\text{III}}\text{C}_{18}\text{H}_{15}\text{O}_{22}^{-2}$ $\text{Fe}_2^{\text{III}}\text{C}_{12}\text{H}_{10}\text{O}_{14}^{-2}$	0.553 0.293 0.152	Iron(III)-citrate (2:2 ; 3:3 Fe: cit) oligomeric complexes. <sup>9,11</sup> 
8.97		230.9234 190.9650 176.9492	$\text{Fe}^{\text{II}}\text{C}_5\text{H}_3\text{O}_7^{-1}$ $\text{Fe}^{\text{II}}\text{C}_4\text{H}_7\text{O}_5^{-1}$ $\text{Fe}^{\text{II}}\text{C}_3\text{H}_5\text{O}_5^{-1}$	0.226 0.583 0.799	

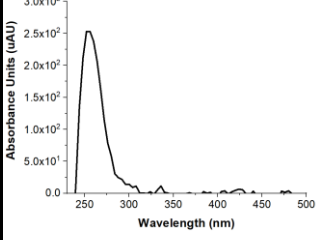
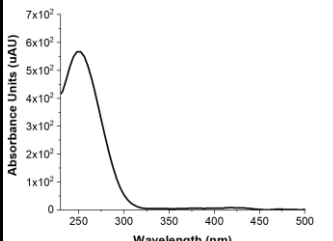
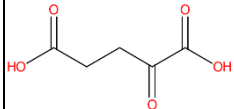
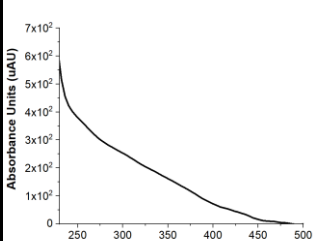
<i>PDA</i> <i>RT (min)</i>	<i>UV-Vis</i> <i>Spectrum</i>	<i>m/z</i>	<i>Ionic, Neutral</i> <i>Formula</i>	<i>Mass</i> <i>Error</i> <i>(ppm)</i>	<i>Proposed</i> <i>Structure &amp; Description</i>
		<i>(-) mode</i>			
<i>40 min Photolysis</i>					
*2.25		115.0038 147.0299 261.0253 246.9553	$\text{C}_4\text{H}_4\text{O}_4$ $\text{C}_5\text{H}_8\text{O}_5$ $\text{C}_9\text{H}_{10}\text{O}_9$ $\text{Fe}^{\text{II}}\text{C}_6\text{H}_7\text{O}_7^{-1}$	0.853 0.200 0.785 2.519	 2-Hydroxypropane-1,2,3-tricarboxylic acid; iron ( $\text{Fe}^{2+}$ ). <sup>13</sup>

2.34		245.0300	$C_9H_{10}O_8$	0.369	
2.43		249.0252	$C_8H_{10}O_9$	0.140	
*2.49		244.9396	$Fe^{II}C_6H_5O_7^{-1}$	1.397	 <p><i>Iron(II)Citrate (1:1 Fe: Cit) based on spectral database match and measured UV-visible spectra.<sup>12</sup></i></p>
*2.6		255.0180 242.9815 173.0093	$Fe^{II}C_6H_{15}O_7^{-1}$ $Fe^{II}C_4H_{11}O_8^{-1}$ $C_6H_6O_6$	1.811 2.747 0.803	

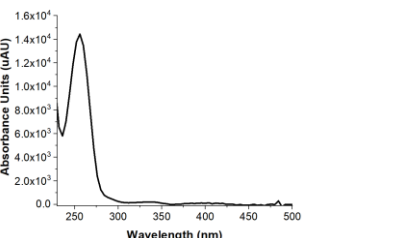
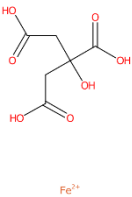
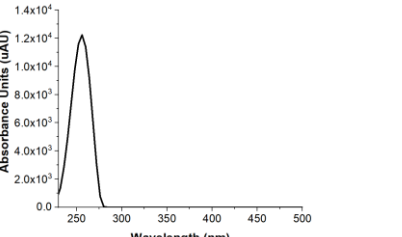
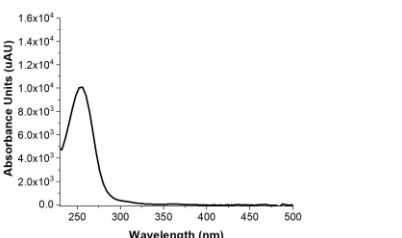
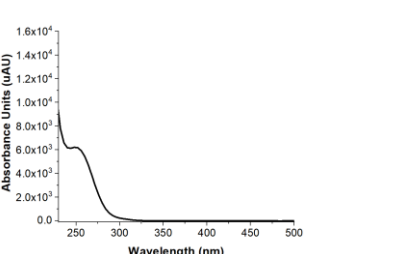
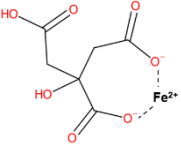
3.12		211.0281 197.0124	$\text{Fe}^{\text{II}}\text{C}_5\text{H}_{15}\text{O}_5^{-1}$ $\text{Fe}^{\text{II}}\text{C}_4\text{H}_{13}\text{O}_5^{-1}$	3.2 3.2	
*6.10		255.0180 211.0281 145.0142	$\text{Fe}^{\text{II}}\text{C}_6\text{H}_{15}\text{O}_7^{-1}$ $\text{Fe}^{\text{II}}\text{C}_5\text{H}_{15}\text{O}_5^{-1}$ $\text{C}_5\text{H}_6\text{O}_5$	0.988 3.2 0.390	<i>α-ketoglutaric acid</i> 
*8.8		230.9234 190.9650 176.9492	$\text{Fe}^{\text{II}}\text{C}_5\text{H}_3\text{O}_7^{-1}$ $\text{Fe}^{\text{II}}\text{C}_4\text{H}_7\text{O}_5^{-1}$ $\text{Fe}^{\text{II}}\text{C}_3\text{H}_5\text{O}_5^{-1}$	1.049 0.897 1.025	

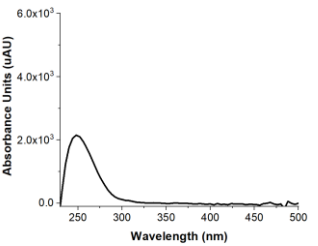
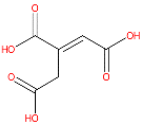
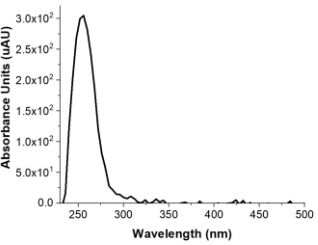
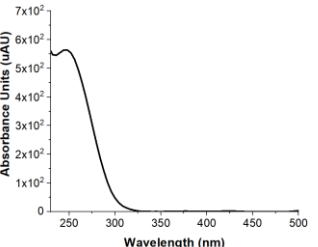
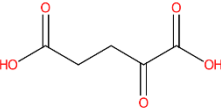
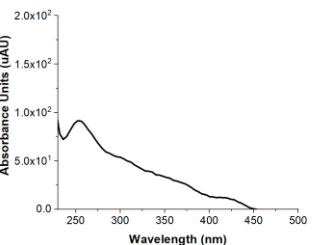
<i>PDA</i> <i>RT (min)</i>	<i>UV-Vis</i> <i>Spectrum</i>	<i>m/z</i>	<i>Ionic, Neutral</i> <i>Formula</i>	<i>Mass</i> <i>Error</i> <i>(ppm)</i>	<i>Proposed</i> <i>Structure</i>
		<i>(-) mode</i>			
<i>80 min Photolysis</i>					

2.25		115.0038 147.0299 231.0146 261.0253 246.9553	$C_4H_4O_4$ $C_5H_8O_5$ $C_8H_8O_8$ $C_9H_{10}O_9$ $Fe^{II}C_6H_7O_7^{-1}$	0.853 0.200 0.431 0.594 2.398	 <p><i>2-Hydroxypropane-1,2,3-tricarboxylic acid; iron (<math>Fe^{2+}</math>).</i><sup>13</sup></p>
2.35		245.0300	$C_9H_{10}O_8$	0.451	
2.46		244.9396	$Fe^{II}C_6H_5O_7^{-1}$	1.479	 <p><i>Iron(II) Citrate (1:1 Fe: Cit) based on spectral database match and measured UV-visible spectra.</i><sup>12</sup></p>
2.58		255.0180 242.9817 173.0093	$Fe^{II}C_6H_{15}O_7^{-1}$ $Fe^{II}C_4H_{11}O_8^{-1}$ $C_6H_6O_6$	2.046 3.529 0.803	

3.12		211.0281 197.0124	$\text{Fe}^{\text{II}}\text{C}_5\text{H}_{15}\text{O}_5^{-1}$ $\text{Fe}^{\text{II}}\text{C}_4\text{H}_{13}\text{O}_5^{-1}$	3.2 3.2	
6.2		255.0180 211.0281 145.0142	$\text{Fe}^{\text{II}}\text{C}_6\text{H}_{15}\text{O}_7^{-1}$ $\text{Fe}^{\text{II}}\text{C}_5\text{H}_{15}\text{O}_5^{-1}$ $\text{C}_5\text{H}_6\text{O}_5$	2.007 3.2 0.369	
8.8		230.9234 190.9650 176.9492	$\text{Fe}^{\text{II}}\text{C}_5\text{H}_3\text{O}_7^{-1}$ $\text{Fe}^{\text{II}}\text{C}_4\text{H}_7\text{O}_5^{-1}$ $\text{Fe}^{\text{II}}\text{C}_3\text{H}_5\text{O}_5^{-1}$	1.006 0.845 1.138	

<i>PDA</i> <i>RT (min)</i>	<i>UV-Vis</i> <i>Spectrum</i>	<i>m/z</i>	<i>Ionic, Neutral</i> <i>Formula</i>	<i>Mass</i> <i>Error</i> <i>(ppm)</i>	<i>Proposed</i> <i>Structure</i>
		<i>(-) mode</i>			
<i>120 min Photolysis</i>					

2.21		115.0038 147.0299 231.0146 261.0253 246.9553	$C_4H_4O_4$ $C_5H_8O_5$ $C_8H_8O_8$ $C_9H_{10}O_9$ $Fe^{II}C_6H_7O_7^{-1}$	0.853 0.200 0.478 0.517 1.547	 <p><i>2-Hydroxypropane-1,2,3-tricarboxylic acid; iron (<math>Fe^{2+}</math>) based on spectral database.<sup>13</sup></i></p>
2.26		231.0146 261.0253 245.0302	$C_8H_8O_8$ $C_9H_{10}O_9$ $C_9H_{10}O_8$	0.478 0.517 0.451	
2.34		245.0302 207.0147	$C_9H_{10}O_8$ $C_6H_8O_8$	0.451 0.384	
2.43		244.9396 241.0023 249.0253 219.0100	$Fe^{II}C_6H_5O_7^{-1}$ $Fe^{II}C_5H_{13}O_7^{-1}$ $C_8H_{10}O_9$ $C_7H_8O_8$	1.723 2.829 0.381 0.592	 <p><i>Iron(II)Citrate (1:1 Fe: Cit) based on spectral database match and measured UV-visible spectra.<sup>12</sup></i></p>

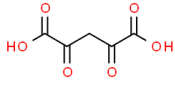
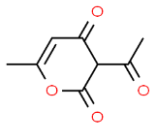
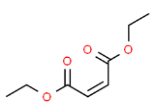
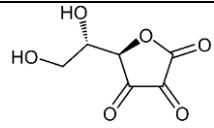
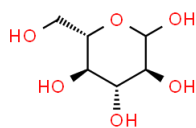
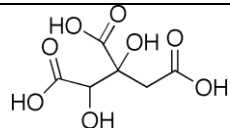
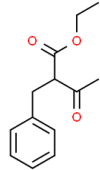
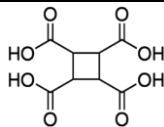
2.58		255.0180 242.9815 173.0093	$\text{Fe}^{\text{II}}\text{C}_6\text{H}_{15}\text{O}_7^{-1}$ $\text{Fe}^{\text{II}}\text{C}_4\text{H}_{11}\text{O}_8^{-1}$ $\text{C}_6\text{H}_6\text{O}_6$	2.007 2.747 0.803	
3.12		211.0281 197.0124	$\text{Fe}^{\text{II}}\text{C}_5\text{H}_{15}\text{O}_5^{-1}$ $\text{Fe}^{\text{II}}\text{C}_4\text{H}_{13}\text{O}_5^{-1}$	3.2 3.2	
6.2		145.0142 211.0281 255.0180	$\text{C}_5\text{H}_6\text{O}_5$ $\text{Fe}^{\text{II}}\text{C}_5\text{H}_{15}\text{O}_5^{-1}$ $\text{Fe}^{\text{II}}\text{C}_6\text{H}_{15}\text{O}_7^{-1}$	0.390 3.133 1.811	
8.8		230.9234 190.9650 176.9492	$\text{Fe}^{\text{II}}\text{C}_5\text{H}_3\text{O}_7^{-1}$ $\text{Fe}^{\text{II}}\text{C}_4\text{H}_7\text{O}_5^{-1}$ $\text{Fe}^{\text{II}}\text{C}_3\text{H}_5\text{O}_5^{-1}$	1.006 -1.172 0.501	

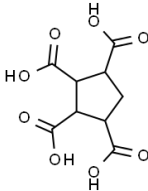
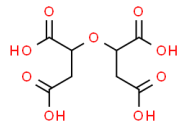
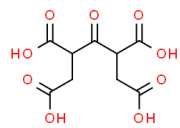
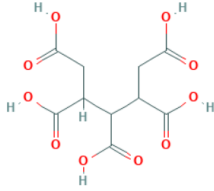
**Table S2:** List of m/z values and ion formulas for Fe- organic complexes and Fe isotopes detected via direct infusion-HRMS for Fe(III)citrate in the form of Fe(III) perchlorate/citric acid and ferric citrate reagent standard, respectively.

<b>m/z (Exp.)</b>	<b>Ion Formula</b>	<b>Error (ppm)</b>	<b>Charge (z)</b>	<b>M:L</b>	<b>Detected Mixture/ Standard</b>
217.4755	$[\text{}^{56}\text{FeC}_{12}\text{H}_{11}\text{O}_{14}]^{2-}$	0.003	2	1:2	Y/Y
243.9313	$[\text{}^{56}\text{Fe}_2\text{C}_{12}\text{H}_8\text{O}_{14}]^{2-}$	0.234	2	2:2	Y/Y
241.9363	$[\text{}^{54}\text{Fe}_2\text{C}_{12}\text{H}_8\text{O}_{14}]^{2-}$	1.713	2	2:2	Y/Y
261.9416	$[\text{}^{56}\text{FeC}_6\text{H}_6\text{O}_8]^-$	0.296	1	1:1	Y/Y
259.9465	$[\text{}^{54}\text{FeC}_6\text{H}_6\text{O}_8]^-$	0.230	1	1:1	Y/Y
271.8988	$[\text{}^{56}\text{Fe}_3\text{C}_{12}\text{H}_{10}\text{O}_{14}]^{2-}$	0.758	2	3:2	Y/Y
279.9078	$[\text{}^{56}\text{Fe}_4\text{C}_{21}\text{H}_{12}\text{O}_{22}]^{3-}$	0.244	3	4:3	Y/Y
366.4005	$[\text{}^{56}\text{Fe}_3\text{C}_{18}\text{H}_{13}\text{O}_{21}]^{2-}$	0.498	2	3:3	Y/Y
363.4081	$[\text{}^{54}\text{Fe}_3\text{C}_{18}\text{H}_{13}\text{O}_{21}]^{2-}$	1.715	2		Y/Y
375.4059	$[\text{}^{56}\text{Fe}_3\text{C}_{18}\text{H}_{15}\text{O}_{22}]^{2-}$	0.586	2	3:3	Y/Y
372.4109	$[\text{}^{54}\text{Fe}_3\text{C}_{18}\text{H}_{15}\text{O}_{22}]^{2-}$	4.884	2		Y/Y
435.9585	$[\text{}^{56}\text{FeC}_{12}\text{H}_{12}\text{O}_{14}]^-$	0.837	1	1:2	Y/Y
462.4145	$[\text{}^{56}\text{Fe}_3\text{C}_{24}\text{H}_{21}\text{O}_{28}]^{2-}$	1.516	2	3:4	Y/N
488.8702	$[\text{}^{56}\text{Fe}_2\text{C}_{12}\text{H}_9\text{O}_{14}]^-$	0.998	1	2:2	Y/Y
484.8795	$[\text{}^{54}\text{Fe}_2\text{C}_{12}\text{H}_9\text{O}_{14}]^-$	1.098	1		Y/Y

**Table S3:** List of m/z values, neutral formulas, double bond equivalency (DBE), and tentative compound associated with water-soluble CHO-containing analytes identified in this study.

<i>m/z (Exp.)</i>	<i>Formula</i>	<i>Tentative Identification</i>	<i>DBE</i>	<i>Structure</i>
101.0245	C <sub>4</sub> H <sub>6</sub> O <sub>3</sub>	Acetoacetic acid	2	
103.0038	C <sub>3</sub> H <sub>4</sub> O <sub>4</sub>	Malonic acid	2	
105.0194	C <sub>3</sub> H <sub>6</sub> O <sub>4</sub>	Glyceric acid	1	
112.9882	C <sub>4</sub> H <sub>2</sub> O <sub>4</sub>	Squaric acid	4	
115.0038	C <sub>4</sub> H <sub>4</sub> O <sub>4</sub>	Fumaric acid	3	
129.0193	C <sub>5</sub> H <sub>6</sub> O <sub>4</sub>	Acetopyruvic acid	3	
143.0349	C <sub>6</sub> H <sub>8</sub> O <sub>4</sub>	Dimethyl-fumaric acid	3	
144.9774	C <sub>4</sub> H <sub>2</sub> O <sub>6</sub>	Dioxosuccinic acid	4	
145.0143	C <sub>5</sub> H <sub>6</sub> O <sub>5</sub>	α-ketoglutaric acid	3	
147.0299	C <sub>5</sub> H <sub>8</sub> O <sub>5</sub>	Citramalic acid	2	

158.9932	$C_5H_4O_6$	2,4-Dioxopentanedioic acid	4	
167.0348	$C_8H_8O_4$	Dehydroacetic acid	5	
171.0664	$C_8H_{12}O_4$	Diethyl fumarate	3	
173.0091	$C_6H_6O_6$	Dehydroascorbic acid	4	
179.0562	$C_6H_{12}O_6$	L-glucopyranose	1	
207.0147	$C_6H_8O_8$	Hydroxycitric acid	3	
219.0146	$C_7H_8O_8$	Propane-tetracarboxylic acid	4	
219.1029	$C_{13}H_{16}O_3$	Benzene propanoic acid	6	
231.0146	$C_8H_8O_8$	Cyclobutane-tetracarboxylic acid	5	

245.0300	$C_9H_{10}O_8$	Cyclopentane-tetracarboxylic acid	5	
249.0253	$C_8H_{10}O_9$	Oxydisuccinic acid <sup>14</sup>	4	
261.0253	$C_9H_{10}O_9$	3-Oxo-1,2,4,5-pentanetetracarboxylic acid <sup>15</sup>	5	
291.0361	$C_{10}H_{12}O_{10}$	Pentane-1,2,3,4,5-pentacarboxylic acid <sup>16</sup>	5	

## References:

- (1) Lehoczki, T.; Józsa, É.; Ósz, K. Ferrioxalate Actinometry with Online Spectrophotometric Detection. *J. Photochem. Photobiol. Chem.* **2013**, *251*, 63–68. <https://doi.org/10.1016/j.jphotochem.2012.10.005>.
- (2) Agustina, E.; Goak, J.; Lee, S.; Seo, Y.; Park, J.-Y.; Lee, N. Simple and Precise Quantification of Iron Catalyst Content in Carbon Nanotubes Using UV/Visible Spectroscopy. *ChemistryOpen* **2015**, *4* (5), 613–619. <https://doi.org/10.1002/open.201500096>.
- (3) Hasegawa, Y.; Takahashi, K.; Kume, S.; Nishihara, H. Complete Solid State Photoisomerization of Bis(Dipyrazolylstyrylpyridine)Iron(II) to Change Magnetic Properties. *Chem. Commun.* **2011**, *47* (24), 6846. <https://doi.org/10.1039/c1cc11850a>.
- (4) Bertoli, A. C.; Carvalho, R.; Freitas, M. P.; Ramalho, T. C.; Mancini, D. T.; Oliveira, M. C.; de Varennes, A.; Dias, A. Structural Determination of Cu and Fe–Citrate Complexes: Theoretical Investigation and Analysis by ESI-MS. *J. Inorg. Biochem.* **2015**, *144*, 31–37. <https://doi.org/10.1016/j.jinorgbio.2014.12.008>.
- (5) N, B.; Md, E.; K, G. Identification of Complexes Containing Glutathione with As(III), Sb(III), Cd(II), Hg(II), Tl(I), Pb(II) or Bi(III) by Electrospray Ionization Mass Spectrometry. *J. Inorg. Biochem.* **2005**, *99* (10), 1992–1997. <https://doi.org/10.1016/j.jinorgbio.2005.06.019>.
- (6) Keith-Roach, M. J. A Review of Recent Trends in Electrospray Ionisation-Mass Spectrometry for the Analysis of Metal-Organic Ligand Complexes. *Anal. Chim. Acta* **2010**, *678* (2), 140–148. <https://doi.org/10.1016/j.aca.2010.08.023>.
- (7) Tsednee, M.; Huang, Y.-C.; Chen, Y.-R.; Yeh, K.-C. Identification of Metal Species by ESI-MS/MS through Release of Free Metals from the Corresponding Metal-Ligand Complexes. *Sci. Rep.* **2016**, *6* (1), 26785. <https://doi.org/10.1038/srep26785>.
- (8) Silva, A. M. N.; Kong, X.; Parkin, M. C.; Cammack, R.; Hider, R. C. Iron(II) Citrate Speciation in Aqueous Solution. *Dalton Trans.* **2009**, No. 40, 8616. <https://doi.org/10.1039/b910970f>.
- (9) Gautier-Luneau, I.; Merle, C.; Phanon, D.; Lebrun, C.; Biaso, F.; Serratrice, G.; Pierre, J.-L. New Trends in the Chemistry of Iron(III) Citrate Complexes: Correlations between X-Ray Structures and Solution Species Probed by Electrospray Mass Spectrometry and Kinetics of Iron Uptake from Citrate by Iron Chelators. *Chem. – Eur. J.* **2005**, *11* (7), 2207–2219. <https://doi.org/10.1002/chem.200401087>.
- (10) Esteban-Fernández, D.; El-Khatib, A. H.; Moraleja, I.; Gómez-Gómez, M. M.; Linscheid, M. W. Bridging the Gap between Molecular and Elemental Mass Spectrometry: Higher Energy Collisional Dissociation (HCD) Revealing Elemental Information. *Anal. Chem.* **2015**, *87* (3), 1613–1621. <https://doi.org/10.1021/ac5032447>.

- (11) Silva, A. M. N.; Kong, X.; Parkin, M. C.; Cammack, R.; Hider, R. C. Iron(III) Citrate Speciation in Aqueous Solution. *Dalton Trans.* **2009**, No. 40, 8616–8625.  
<https://doi.org/10.1039/B910970F>.
- (12) National Center for Biotechnology Information. “PubChem Compound Summary for CID 14298643, Ferrous Citrate” PubChem,  
<https://pubchem.ncbi.nlm.nih.gov/compound/Ferrous-Citrate>. Accessed 18 December, 2020.
- (13) National Center for Biotechnology Information. “PubChem Compound Summary for CID 31889, 2-Hydroxypropane-1,2,3-Tricarboxylic Acid;Iron(2+)” PubChem,  
<https://pubchem.ncbi.nlm.nih.gov/compound/31889>. Accessed 18 December, 2020.
- (14) PubChem. Oxydisuccinic acid, (+/-)-  
<https://pubchem.ncbi.nlm.nih.gov/compound/90479035> (accessed 2021 -11 -09).
- (15) 3-Oxo-1,2,4,5-pentametetracarboxylic acid | C<sub>9</sub>H<sub>10</sub>O<sub>9</sub> | ChemSpider  
<http://www.chemspider.com/Chemical-Structure.9405827.html> (accessed 2021 -11 -09).
- (16) PubChem. Pentane-1,2,3,4,5-pentacarboxylic acid  
<https://pubchem.ncbi.nlm.nih.gov/compound/21915725> (accessed 2021 -11 -09).